

## PROCESS OPTIMIZATION FOR THE FRONT SIDE OF P-TYPE SILICON SOLAR CELLS

S. Werner, E. Lohmüller, S. Maier, A. Kimmerle, A. Spribille, S. Wasmer, F. Clement, A. Wolf  
 Fraunhofer Institute for Solar Energy Systems ISE, Heidenhofstraße 2, 79110 Freiburg, Germany  
 Phone: +49 761 - 4588 5049, e-mail: sabrina.werner@ise.fraunhofer.de

**ABSTRACT:** In this work, we optimize the front side of p-type Czochralski-grown silicon (Cz-Si) solar cells by investigating industrial-type phosphorus diffusion processes, and by adapting the front-side metallization. The utilization of a metallization grid with less coverage, combined with double printing, results in an increase in conversion efficiency  $\eta$  of 0.5 %<sub>abs</sub> for p-type Cz-Si H-pattern cells with aluminium back surface field. By incorporating *in-situ* oxidation into the diffusion process, we realize a surface doping concentration of  $\approx 2 \cdot 10^{20} \text{ cm}^{-3}$  for our improved emitter. With this diffusion process, a low emitter dark saturation current density of  $85 \text{ fA/cm}^2$  is achieved while maintaining low specific contact resistance  $\leq 4 \text{ m}\Omega\text{cm}^2$ . The application of this emitter results in a gain in  $\eta$  of 0.4 %<sub>abs</sub> for p-type Cz-Si high-performance metal wrap trough (HIP-MWT) solar cells in comparison to a diffusion process without *in-situ* oxidation. For the best performing HIP-MWT cell,  $\eta$  reaches 20.5 %. Furthermore, we test the stability and reproducibility of our improved diffusion process in ten runs with 200 wafers each. The mean sheet resistance is found to be  $(85 \pm 2) \Omega/\text{sq}$ , revealing high homogeneity over full-load runs.

**Keywords:** passivation, phosphorus doping,  $\text{POCl}_3$  diffusion, metallization, silicon solar cell

## 1 INTRODUCTION

The optimization of diffusion processes and the resulting doping profiles are essential for further increasing the conversion efficiency of silicon solar cells. For p-type silicon solar cells, the phosphorus emitter is typically formed by tube furnace gas diffusion using phosphorus oxychloride ( $\text{POCl}_3$ ). In order to achieve higher open-circuit voltages  $V_{\text{OC}}$ , the emitter dark saturation current density of the passivated diffused surfaces  $j_{\text{oe}}$  needs to be decreased. As a means of achieving this, the surface doping concentration  $N_{\text{S}}$  should be reduced. However, at the same time, low specific contact resistances  $\rho_{\text{c}}$  need to be ensured for screen-printed metallization. To meet these requirements, selective emitters have been developed [1] by implementing different technologies, which have at least one additional process step in common [2]. As the current generation of screen printing silver pastes allows contacting of phosphorus-doped emitters with  $N_{\text{S}}$  in the range of 1 to  $2 \cdot 10^{20} \text{ cm}^{-3}$ —while maintaining low  $\rho_{\text{c}}$  values [3,4]—utilizing novel emitter doping profiles without the need for the selective emitter technology is possible.

Apart from  $j_{\text{oe}}$  of the passivated front surface, also the saturation current density  $j_{\text{omet}}$  underneath the metal contacts impacts  $V_{\text{OC}}$ . One option to reduce the impact of  $j_{\text{omet}}$  is to decrease the contacted area. This can be achieved by using a metal wrap through (MWT) cell structure [5], such as the high-performance MWT (HIP-MWT) concept [6,7], for example.

## 2 APPROACH

In the first part of this work, industrial-type  $\text{POCl}_3$  diffusion processes are investigated, aiming to reduce  $j_{\text{oe}}$  and increase  $V_{\text{OC}}$ , while maintaining a high blue response, a reasonable sheet resistance, and low  $\rho_{\text{c}}$  for screen-printed metallization. An option to decrease  $N_{\text{S}}$  is the use of a thermal oxidation process. This thermal oxidation can either be performed in an additional high-temperature step [8] or incorporated into the  $\text{POCl}_3$  diffusion process for less process complexity [9–13].

Throughout this work, an industrial automated high-throughput (200 slots per boat) atmospheric pressure tube

furnace is used for the high-temperature steps. The  $\text{POCl}_3$  diffusion processes investigated in this work are initially characterized by measuring  $j_{\text{oe}}$  on symmetric lifetime-samples with textured surfaces. Subsequently, the most promising emitters are evaluated on cell level. Therefore, p-type Czochralski-grown silicon (Cz-Si) HIP-MWT solar cells are fabricated in the industry-related PV-TEC pilot line at Fraunhofer ISE [14]. The stability and reproducibility of the most promising  $\text{POCl}_3$  diffusion process is also tested in ten diffusion runs with 200 wafers each to make sure that the full boat can be used which is of relevance for industrial feasibility of all developed processes.

In the second part of this work, the front side metallization pattern is adapted on p-type Cz-Si solar cells with aluminum back surface field (Al-BSF). For this, tapered busbars are used, which result in higher short-circuit current densities  $j_{\text{SC}}$  and reduced silver paste consumption. By the integration of double-printing, the limitation due to the finger grid is investigated as well.

3  $\text{POCl}_3$  DIFFUSION PROCESS DEVELOPMENT

## 3.1 Investigated process sequences

The different  $\text{POCl}_3$  diffusion processes investigated in this work are summarized in Table I. The process DiffRef is the initial  $\text{POCl}_3$  diffusion process without *in-situ* oxidation and serves as a reference. After the deposition phase with  $\text{POCl}_3$ ,  $\text{O}_2$ , and  $\text{N}_2$ , the drive-in phase follows with  $\text{N}_2$  as the only ambient gas at the same temperature. Emitter DiffSubOx is formed using two separate high-temperature processes. First, the doped

**Table I:** Summary of the  $\text{POCl}_3$  diffusion processes investigated in this work.

Emitter	$\text{POCl}_3$ diffusion process
DiffRef	Reference diffusion
DiffSubOx	Diffusion with subsequent separate thermal oxidation
DiffOxFlat	Diffusion with <i>in-situ</i> oxidation 1
DiffOxDeep	Diffusion with <i>in-situ</i> oxidation 2
DiffOxImp	Diffusion with <i>in-situ</i> oxidation 3

surfaces are formed in a diffusion process similar to the one used for emitter DiffRef. After removal of the phosphosilicate glass layer (PSG) and wet-chemical cleaning, a thermal oxidation is performed to decrease  $N_S$  and to drive in the phosphorus dopants. For diffusion processes DiffOxFlat, DiffOxDeep, and DiffOxImp, the oxidation step is incorporated into the drive-in step of the diffusion process and carried out at higher temperatures than the deposition step. All processes differ in peak temperatures, gas flow rates, and process times. Hence, the resulting emitter sheet resistances  $R_{sh}$ , measured by means of inductive coupling [15] are different and range from 55  $\Omega/\text{sq}$  to 92  $\Omega/\text{sq}$ .

### 3.2 Doping profiles

The respective charge carrier concentration profiles in Fig. 1 are measured by electrochemical capacitance-voltage (ECV) profiling [16] on alkaline saw-damage-etched surfaces. The doping profiles differ in  $N_S$  (2.1 to  $3.4 \cdot 10^{20} \text{ cm}^{-3}$ ) and depth  $d$  (350 to 700 nm at a dopant concentration  $N = 10^{16} \text{ cm}^{-3}$ ). Diffusion process DiffOxDeep features a longer *in-situ* oxidation phase at a higher temperature than process DiffOxFlat, resulting in a significantly deeper profile. Due to this deeper profile, process DiffOxDeep shows a lower  $j_{sc}$ . Thus, for the improved process DiffOxImp, the *in-situ* oxidation is optimized with regard to a comparably low  $N_S$  as well as a lower junction depth  $d$  compared to emitter DiffOxDeep. However, the doping profile of process DiffOxDeep is very interesting for the phosphorus-doped BSF of n-type silicon solar cells and is applied for such solar cells in ref. [17].

As ECV measurements only detect electrically active phosphorus, the doping profiles in Fig. 1 comprise no existing electrically inactive phosphorus. The equilibrium concentration  $n_e$  of the electrically active dopants can be calculated as a function of the peak temperature achieved during the high-temperature process [18]. Based on these calculations, no electrically inactive phosphorus is expected for the processes DiffOxDeep and DiffOxImp. However, the measured  $N_S$  of DiffRef and DiffOxFlat unreasonably exceed the calculated  $n_e$ .

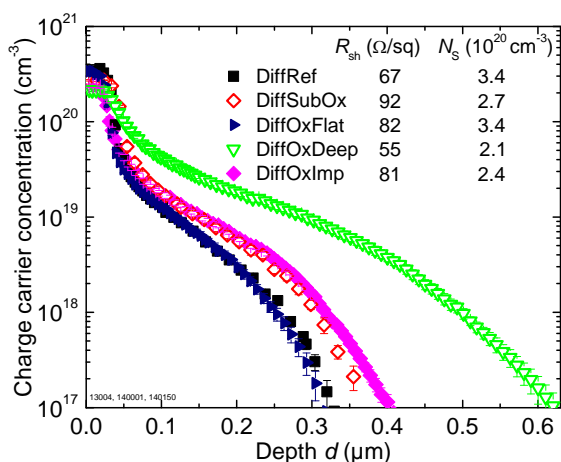


**Figure 1:** Charge carrier concentration profiles, determined by ECV measurements on alkaline saw-damage-etched surfaces, of the five investigated  $\text{POCl}_3$  diffusion processes. The surface doping concentrations  $N_S$  and emitter sheet resistances  $R_{sh}$  are also stated. The latter are measured by means of inductive coupling [15].

### 3.3 Emitter dark saturation current densities $j_{0e}$

To determine  $j_{0e}$  of the different emitters on textured surfaces, symmetric n-type Cz-Si lifetime samples (three for each emitter) with an edge length of 156 mm and a specific base resistance of  $\rho_{base} \approx 6 \Omega\text{cm}$  are fabricated.

After  $\text{POCl}_3$  diffusion, the PSG is removed and silicon nitride anti-reflective coating ( $\text{SiN}_x$ -ARC) is deposited onto both surfaces by plasma-enhanced chemical vapor deposition. For the samples with emitter DiffSubOx, the thin thermal oxide layer on both sides is kept for improved surface passivation. For all samples, the  $\text{SiN}_x$ -ARC layer thickness is adapted such that the minimum reflection of the samples—with or without thermal oxide—is measured at a wavelength of  $\approx 600 \text{ nm}$ . For fast firing, the set temperature is lowered for the lifetime samples compared to metallized solar cells in order to reach similar peak wafer temperatures.

Finally, quasi steady state photo conductance (QSSPC) measurements yield the effective lifetime at five points for each sample. Then,  $j_{0e}$  is obtained by applying the  $j_0$ -analysis as in the Sinton Instruments' WCT-120 [19]. Fig. 2 shows the determined  $j_{0e}$  values of the five investigated  $\text{POCl}_3$  diffusion processes. The open-circuit voltage limit  $V_{OC,limit}$  can be found from  $j_{0e}$  by using the one-diode model with  $j_{sc} = 39 \text{ mA}/\text{cm}^2$  and temperature  $T = 25^\circ\text{C}$ .

The reference diffusion process DiffRef leads to an  $R_{sh} \approx 69 \Omega/\text{sq}$  and a  $j_{0e} \approx 259 \text{ fA}/\text{cm}^2$ . The additional oxidation step for process DiffSubOx decreases the amount of electrically inactive phosphorus and leads to a deeper pn-junction. It results in  $R_{sh} \approx 92 \Omega/\text{sq}$  and a decreased  $j_{0e}$  of  $\approx 158 \text{ fA}/\text{cm}^2$ . Process DiffOxFlat yields very similar  $R_{sh}$  and  $j_{0e}$  values as process DiffSubOx, but features only a  $\text{SiN}_x$  passivation layer and no additional process steps are necessary. DiffOxDeep with a longer *in-situ* oxidation at a higher temperature results in a deeper profile and lowered  $N_S$ . The values for this process are  $R_{sh} \approx 62 \Omega/\text{sq}$  and  $j_{0e} \approx 112 \text{ fA}/\text{cm}^2$ .

For DiffOxImp, process parameters are adjusted such that  $N_S$  is similar to that of DiffOxDeep, while the dopants are less deeply driven in. Thus, emitter DiffOxImp features a higher  $R_{sh} \approx 93 \Omega/\text{sq}$  and a lower

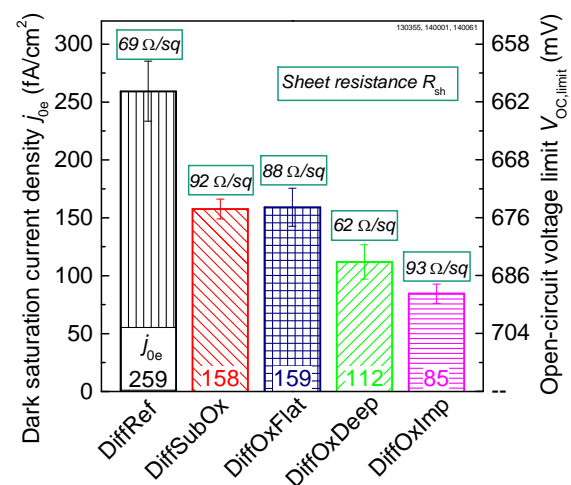


**Figure 2:** Left axis: emitter dark saturation current density  $j_{0e}$ . Right axis: open-circuit voltage limit  $V_{OC,limit}$ . The error bars represent the standard deviation of  $j_{0e}$  measured on three samples at five positions each. The emitter sheet resistances  $R_{sh}$ , measured for the symmetric lifetime samples, are stated in the gray boxes.

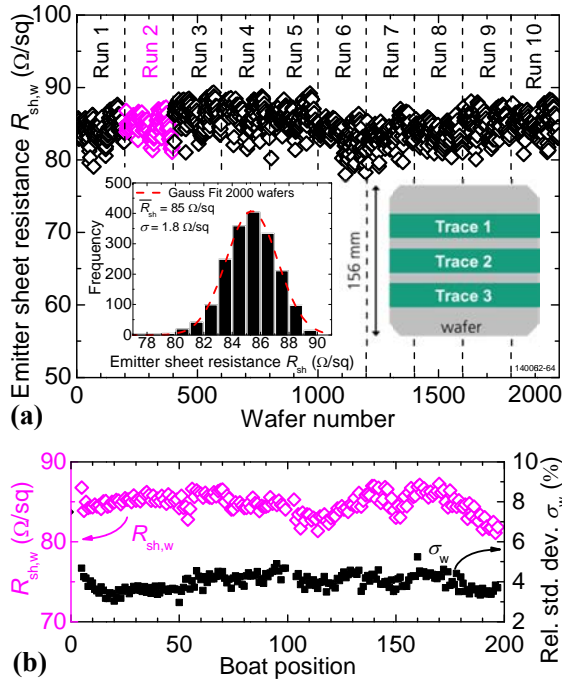


**Figure 3:** (a) Emitter sheet resistances  $R_{sh,w}$  of ten runs with 200 wafers each for diffusion process DiffOxImp.  $R_{sh,w}$  is determined with an inline tool on three traces over the wafer by means of inductive coupling. The inset shows the Gaussian distribution of the 2000  $R_{sh,w}$  values illustrating the boat uniformity. (b)  $R_{sh,w}$  and relative wafer standard deviation  $\sigma_w$  exemplarily for Run 2 (full-load).

$j_{0e} \approx 85 \text{ fA/cm}^2$  compared with emitter DiffOxDeep. This emitter allows for a  $V_{OC,limit} \approx 690 \text{ mV}$ , resulting in an increase of almost 30 mV in  $V_{OC,limit}$  with respect to the reference emitter DiffRef.

### 3.4 Stability and reproducibility of the improved $\text{POCl}_3$ diffusion process DiffOxImp

For testing the stability and reproducibility of the improved diffusion process DiffOxImp, ten runs with 200 wafers each (full boat) are performed. The front sides of the wafers are alkaline textured, whereas the alkaline saw-damage-etched rear side is covered with a thermal oxide layer serving as diffusion barrier.

The emitter sheet resistances, determined for every single wafer  $w$  ( $R_{sh,w}$ ) by means of inductive coupling [15], are summarized in Fig. 3 (a). Three sensors  $s$  with a diameter of 25 mm and a wafer-to-wafer distance of 35 mm are used measure  $R_{sh,w}$ . Every sensor records 25 measurement points  $p$  ( $R_{sh,s,p}$ ) on a trace parallel to the wafer edge. The mean emitter sheet resistance for a single wafer calculates to

$$R_{sh,w} = \frac{1}{75} \left( \sum_{s=1}^3 \sum_{p=1}^{25} R_{sh,s,p} \right).$$

The measured  $R_{sh,w}$  values for the 2000 wafers show a Gaussian distribution with a mean value

$$\bar{R}_{sh} = \frac{1}{2000} \left( \sum_{i=1}^{2000} R_{sh,w_i} \right) \approx 85 \text{ } \Omega/\text{sq},$$

and a standard deviation  $\sigma \approx 2 \text{ } \Omega/\text{sq}$ . The relative standard deviation

$$\sigma_w = \frac{\sqrt{\frac{1}{75} \sum_{s=1}^3 \sum_{p=1}^{25} (R_{sh,s,p} - R_{sh,w})^2}}{R_{sh,w}}$$

is defined as the standard deviation of all measured  $R_{sh,s,p}$  values of a single wafer relative to the wafer emitter sheet resistance  $R_{sh,w}$ . Fig. 3 (b) shows exemplarily the  $\sigma_w$  values for every wafer of Run 2, which is representative for all runs. The mean  $\sigma_w$  of all 2000 measured wafers calculates to  $\bar{\sigma}_w \approx 4 \%$ .

These results show the high homogeneity achieved over the fully-loaded boats as well as over the single wafers for the improved diffusion process DiffOxImp.

## 4 EMITTER COMPARISON ON CELL LEVEL

### 4.1 Fabrication of HIP-MWT solar cells

To compare the different  $\text{POCl}_3$  diffusion processes on cell level, HIP-MWT solar cells are fabricated according to the process sequence shown in ref. [20]. Full-square p-type Cz-Si wafers with an edge length of 156 mm, an initial thickness of  $t \approx 200 \text{ } \mu\text{m}$ , and  $\rho_{base}$  ranging from 1  $\Omega\text{cm}$  to 3  $\Omega\text{cm}$  serve as base material. A thermally grown oxide layer is used as a diffusion barrier during emitter formation and later as the rear-side passivation.

A batch of cells is processed using four of the five diffusion processes: DiffRef, DiffOxFlat, DiffOxDeep, and DiffOxImp. After measuring the current-voltage ( $I$ - $V$ ) characteristics,  $\rho_c$  is determined on two selected cells for each emitter. Therefore, transfer-length method (TLM, [21]) measurements are performed at twelve different positions per cell. Furthermore, the internal quantum efficiency (IQE) is measured in order to analyze the influence of the different emitters on the blue response of the solar cells.

### 4.2 Current-voltage data of the HIP-MWT cells

The results of the  $I$ - $V$  measurements of the fabricated p-type Cz-Si HIP-MWT solar cells with the different emitters are summarized in Table II.

Having a median peak conversion efficiency of  $\eta = 19.6 \%$ , the cells with the improved emitter DiffOxImp clearly outperform the cells with reference emitter DiffRef and  $\eta = 19.2 \%$ . This increase in  $\eta$  of 0.4 %<sub>abs</sub> originates from an increase in  $V_{OC}$  (+9 mV) and  $j_{sc}$  (+0.4 mA/cm<sup>2</sup>).

**Table II:** Median  $I$ - $V$  data of the fabricated p-type Cz-Si HIP-MWT solar cells for the different emitters. The measurements are performed with an industrial cell tester directly after processing. The group size is indicated in brackets. The specific contact resistances  $\rho_c$  are measured on two cells per group (mean value is stated).

Emitter	$\eta$ (%)	$V_{OC}$ (mV)	$j_{sc}$ (mA/cm <sup>2</sup> )	FF (%)	$r_s$ ( $\Omega\text{cm}^2$ )	$\rho_c$ ( $\text{m}\Omega\text{cm}^2$ )
DiffRef (7)	19.2	636	39.3	76.8	1.06	1.4
DiffOxFlat (6)	19.4	639	39.7	76.3	1.08	2.9
DiffOxDeep (8)	19.2	641	38.8	77.3	1.02	1.2
DiffOxImp (7)	19.6	645	39.7	76.3	1.15	4.1

**Table III:** The difference in  $j_{SC}$  for the emitters is stated relative to emitter DiffRef. The difference  $\Delta j_{SC}$ , which is caused by the emitter, is calculated from IQE measurements as described in ref. [22]. The values refer to mean values of two cells per emitter.

Emitter	$\Delta j_{SC}$ rel. to DiffRef (mA/cm <sup>2</sup> )	
	<i>I-V</i> data	IQE (emitter only)
DiffRef	0	0
DiffOxFlat	+ 0.4	+ 0.2
DiffOxDeep	- 0.5	- 0.4
DiffOxImp	+ 0.4	+ 0.3

In contrast to  $V_{OC,limit}$  indicated in Fig. 2, the  $V_{OC}$  of a real cell also includes contributions from the saturation current densities of the front-side metallization  $j_{0met,front}$ , the base  $j_{0base}$ , and the rear side  $j_{0rear}$ . By applying the two-diode model for the median cells with emitter DiffRef and emitter DiffOxImp, the total  $j_{01}$  for the first diode is found to be  $j_{01,2D} = 637$  fA/cm<sup>2</sup> and  $j_{01,2D} = 458$  fA/cm<sup>2</sup>, respectively. The difference calculates to  $\Delta j_{01,2D} = 179$  fA/cm<sup>2</sup>.

Assuming that the total  $j_{01}$  can be described as the sum of the single recombination paths,

$$j_{01} = j_{0e} \cdot (1 - F_M) + j_{0met,front} \cdot F_M + j_{0base} + j_{0rear}. \quad (1)$$

By further assuming that  $j_{0met,front}$ ,  $j_{0base}$ , and  $j_{0rear}$  are equal for both cells as well as knowing that the front side metal coverage  $F_M = 3.5\%$  is identical, the difference of both cells'  $j_{01}$  is simply the difference of their  $j_{0e}$  multiplied by  $(1 - F_M)$ , which calculates to  $\Delta j_{01} = 169$  fA/cm<sup>2</sup>. This is in good agreement with  $\Delta j_{01,2D} = 179$  fA/cm<sup>2</sup>, determined by fitting the cells' *I-V* data to the two-diode model. Hence, the  $V_{OC}$  gain of 9 mV for the cells with the improved emitter DiffOxImp exhibits the maximum achievable enhancement in  $V_{OC}$  compared to the cells with emitter DiffRef.

The remaining  $j_{0rem}$ —the total  $j_{01}$  without  $j_{0e}$  contributions—calculates to  $j_{0rem} \approx 375$  fA/cm<sup>2</sup>. Thus, due to  $j_{0e} = 85$  fA/cm<sup>2</sup> and  $j_{0rem}$  being more than four times higher, emitter recombination is not the dominating loss factor for  $V_{OC}$  in the case of the cells with emitter DiffOxImp. Cells with emitter DiffOxFlat or DiffOxDeep also show higher  $V_{OC}$  values than the reference emitter DiffRef. As above, similarly performed  $j_{01}$  calculations reveal that the higher  $V_{OC}$  of these cells also fits to their reduced  $j_{0e}$  values.

To determine the emitter contribution on  $j_{SC}$ , IQE measurements are performed and analyzed according to ref. [22]. As Table III shows, the difference in  $j_{SC}$  between the cells is mainly due to a different blue response of the respective emitter. The given values are stated relative to emitter DiffRef. The relative  $j_{SC}$  differences extracted from the *I-V* data as well as from the IQE data follow the same trend. For the cells with improved emitter DiffOxImp, the gain in  $j_{SC}$  is 0.3 mA/cm<sup>2</sup> compared to those with emitter DiffRef. The ones with emitter DiffOxFlat show a similarly large  $j_{SC}$  gain. In contrast, the cells with emitter DiffOxDeep suffer from a significantly lower blue response. With respect to cells with emitter DiffOxImp, the loss in  $j_{SC}$  is 0.7 mA/cm<sup>2</sup>.

The series resistance is found to be rather high for all fabricated cells with  $r_S \approx 1.1 \Omega\text{cm}^2$ . This is also reflected by relatively low fill factors  $FF \leq 77.3\%$ . Since the values for  $\rho_c$  are low for all emitters ( $\rho_c \leq 4.1 \text{ m}\Omega\text{cm}^2$ )

and contribution from the front grid resistance  $r_{S,grid}$  is low as well ( $r_{S,grid} \approx 0.15 \Omega\text{cm}^2$ ), a non-optimum rear-side contact formation is considered to be the reason for the rather high  $r_S$  values. Note that no adaption of the front metallization grid has been performed with respect to the different  $R_{sh}$  values of the different emitters. However,  $\rho_c$  is slightly higher for the improved emitter DiffOxImp, demonstrating further potential for optimization.

As mentioned above, the performance of the fabricated HIP-MWT cells with emitter DiffOxImp is not primarily dominated by  $j_{0e}$ . In a further experiment, we optimized the rear side and achieved a  $V_{OC}$  and  $j_{SC}$  of 660 mV and 40.4 mA/cm<sup>2</sup>, respectively. This results in a peak conversion efficiency of 20.5%. As  $r_S$  is still rather high for these cells ( $r_S \approx 1.1 \Omega\text{cm}^2$ ), further improvement is ongoing.

## 5 ADAPTED FRONT SIDE METALLIZATION

### 5.1 Fabrication of Al-BSF solar cells

The adapted front side metallization is investigated on Al-BSF solar cells. For their fabrication, pseudo-square p-type Cz-Si wafers with an edge length of 156 mm, a diameter of 200 mm, an initial thickness  $t \approx 200 \mu\text{m}$ , and  $\rho_{base} \approx 2 \Omega\text{cm}$  are used. After alkaline texturing, the emitter is formed by using POCl<sub>3</sub> diffusion DiffSubOx. PSG etching, front passivation, and screen printing of the rear-side aluminum contact (including silver soldering pads) followed.

The variations performed for the front side metallization are summarized in Table IV. For these screen printing processes, a commercial silver paste is used. The finger width is measured on various cells and determined to  $w_{fi} \approx 60 \mu\text{m}$  for all groups. In a single screen printing step, the first group of H-pattern cells is metallized by a three-busbar grid consisting of fingers and straight external busbar contacts with 1.5 mm width. For the second group, tapered busbars are used without changing the finger grid layout. This results in a decrease of metallization fraction from  $F_M \approx 6.3\%$  to  $F_M \approx 4.4\%$ . Consequently, the silver paste consumption decreases from  $m_{Ag} \approx 140$  mg to  $m_{Ag} \approx 110$  mg. For the third group, the grid with tapered busbars is printed two times in order to investigate limitations due to the series resistance  $r_S$  caused by the finger structures. Hence, the mean maximum finger height increases from  $h_{Fi} \approx 21 \mu\text{m}$  to  $h_{Fi} \approx 34 \mu\text{m}$ , which improves the aspect ratio by a factor of  $\approx 1.6$ . Since apart the fingers also the busbars are printed twice (not cost optimized procedure), the silver paste laydown is rather high with  $m_{Ag} \approx 76$  mg.

**Table IV:** Metallization fraction  $F_M$  and silver paste consumption  $m_{Ag}$  for the screen printing layouts used for metallization of the Al-BSF cells. All layouts feature the same finger number and finger width (BB = busbar).

Metallization process	Metallization fraction	Silver paste consumption
	$F_M$ (%)	$m_{Ag}$ (mg)
1.5 mm BBs, single print	$\approx 6.3$	$\approx 140$
Tapered BBs, single print	$\approx 4.4$	$\approx 110$
Tapered BBs, double print	$\approx 4.4$	$\approx 110 + 76$

**Table V:** Median  $I$ - $V$  data of the p-type Cz-Si Al-BSF cells fabricated with different screen printing layouts. The  $I$ - $V$  data is measured after 36 hours of illumination at 0.2 suns. The group size is indicated in brackets.

Metallization process	$\eta$ (%)	$V_{OC}$ (mV)	$j_{SC}$ (mA/cm <sup>2</sup> )	$FF$ (%)	$r_s$ ( $\Omega$ cm <sup>2</sup> )
1.5 mm BBs, single print	(8)	18.4	627	37.2	78.8
Tapered BBs, single print	(5)	18.9	627	38.1	78.9
Tapered BBs, double print	(6)	19.1	628	38.1	79.7

## 5.2 Current-voltage data of the Al-BSF cells

The results of the  $I$ - $V$  measurements of the fabricated p-type Cz-Si Al-BSF solar cells with the different screen printing layouts are summarized in Table V.

The utilization of a metallization grid with tapered busbars (less shading) allows for a  $j_{SC}$  gain up to 0.9 mA/cm<sup>2</sup>. With similar  $V_{OC}$  and  $FF$  values, this results in a gain in  $\eta$  of 0.5 %<sub>abs</sub>, while decreasing silver paste consumption by 30 mg (see Table IV). However, no positive effect on  $V_{OC}$  is observed for the layout with tapered busbars and, thus, less metallization fraction. We attribute this to the overall high  $j_{01}$  of these cells ( $j_{01} \approx 850$  fA/cm<sup>2</sup>) and hence, to a negligible impact of the realized lower metallization fraction on  $j_{01}$  on the cells' front side.

The specific contact resistance is found to be  $\rho_c \leq 3.8$  m $\Omega$ cm<sup>2</sup> and thus on a similar level as for the HIP-MWT solar cells. The series resistances  $r_s$  are slightly higher for the cells with tapered busbars compared with the cells with straight busbars. By utilization of double printing for the grid with tapered busbars,  $r_s$  is significantly reduced by  $\approx 0.1$   $\Omega$ cm<sup>2</sup>, resulting in a  $FF$  of 79.7 %. This demonstrates further potential for improvement concerning the decrease of series resistance contributions.

## 6 SUMMARY

We optimize the performance of the front sides of p-type Cz-Si solar cells by improving industrial-type phosphorus diffusion and by adapting the front-side metallization.

The improved diffusion process, that includes an *in-situ* oxidation step, leads to a surface doping concentration  $N_s \approx 2 \cdot 10^{20}$  cm<sup>-3</sup> and a low emitter dark saturation current density of 85 fA/cm<sup>2</sup>. By applying this emitter for p-type Cz-Si high-performance metal wrap through (HIP-MWT) solar cells, a gain in conversion efficiency  $\eta$  of 0.4 %<sub>abs</sub> is achieved in comparison with a diffusion process without *in-situ* oxidation. A maximum  $\eta$  of 20.5 % is demonstrated for a HIP-MWT cell with an improved rear side. The reproducibility of the improved diffusion process is tested in ten runs à 200 wafers each. The standard deviation in sheet resistance of  $\pm 2$   $\Omega$ /sq, resulting from the measurements on the 2000 wafers, shows the high stability and the industrial relevance of this process.

The utilization of a metallization grid with less coverage, combined with double printing, results in an increase of conversion efficiency  $\eta$  of 0.5 %<sub>abs</sub> for p-type Cz-Si H-pattern cells with aluminium back surface field.

## ACKNOWLEDGEMENTS

The authors thank all colleagues at the Fraunhofer ISE PV-TEC; especially U. Belledin, A. Drews, W. Hasan, M. Hendrichs, R. Hoenig, K. Schneider, E. Schäffer, and B. Thaidigsmann. This work was funded by the German Federal Ministry for Economic Affairs and Energy (project "RDEMO", contract number: 0325355; "THESSO", 0325491), and the Baden-Wuerttemberg Stiftung ("MikroSol", U23).

## REFERENCES

- [1] V. E. Lowe, A. C. Day, "High-temperature-stable contact metallization for silicon solar cells", *IEEE Trans. Electron Devices*, vol. 31, no. 5, pp. 626–629, 1984.
- [2] G. Hahn, "Status of selective emitter technology", *Proc. 25th EU PVSEC*, Valencia, Spain, 2010, pp. 1091–1096.
- [3] M. Z. Burrows, A. Meisel, D. Balakrishnan et al., "Front-side silver contacts with improved recombination and fine-line performance", *Proc. 28th EU PVSEC*, Paris, France, 2013, pp. 1985–1988.
- [4] V. Shanmugam, J. Cunnusamy, A. Khanna et al., "Electrical and microstructural analysis of contact formation on lightly doped phosphorus emitters using thick-film Ag screen printing pastes", *IEEE J. Photovoltaics*, vol. 4, no. 1, pp. 168–174, 2014.
- [5] E. Van Kerschaver, R. Einhaus, J. Szlufcik et al., "A novel silicon solar cell structure with both external polarity contacts on the back surface", *Proc. 2nd WCPEC*, Vienna, Austria, 1998, pp. 1479–1482.
- [6] B. Thaidigsmann, F. Clement, A. Wolf et al., "HIP-MWT: A simplified structure for metal wrap through solar cells with passivated rear surface", *Energy Procedia*, vol. 8, pp. 498–502, 2011.
- [7] B. Thaidigsmann, M. Linse, A. Wolf et al., "The path to industrial production of highly efficient metal wrap through silicon solar cells", *Green*, vol. 2, no. 4, pp. 171–176, 2012.
- [8] S. Mack, U. Jäger, G. Kästner et al., "Towards 19% efficient industrial PERC devices using simultaneous front emitter and rear surface passivation by thermal oxidation", *Proc. 25th EU PVSEC*, Valencia, Spain, 2010, pp. 17–21.
- [9] A. Cuevas, "A good recipe to make silicon solar cells", *Proc. 22nd IEEE PVSC*, Las Vegas, USA, 1991, pp. 466–470.
- [10] P. A. Basore, J. M. Gee, M. Buck et al., "Simplified high-efficiency silicon cell processing", *Sol. Energy Mater. Sol. Cells*, vol. 34, no. 1-4, pp. 91–100, 1994.
- [11] Y. Komatsu, G. Galbiati, M. Lamers et al., "Innovative diffusion processes for improved efficiency on industrial solar cells by doping profile manipulation", *Proc. 24th EU PVSEC*, Hamburg, Germany, 2009, pp. 1–5.
- [12] Y. Komatsu, A. Stassen, P. Venema et al., "Sophistication of doping profile manipulation - emitter performance improvement without additional process step", *Proc. 25th EU PVSEC*, Valencia, Spain, 2010, pp. 1924–1929.

- [13] A. Kimmerle, R. Woehl, A. Wolf et al., "Simplified front surface field formation for back contacted silicon solar cells", *Energy Procedia*, vol. 38, pp. 278–282, 2013.
- [14] D. Biro, R. Preu, S. W. Glunz et al., "PV-Tec: Photovoltaic technology evaluation center - design and implementation of a production research unit", *Proc. 21st EU PVSEC*, Dresden, Germany, 2006, pp. 621–624.
- [15] M. Spitz, U. Belledin, S. Rein, "Fast inductive inline measurement of the emitter sheet resistance in industrial solar cell fabrication", *Proc. 22nd EU PVSEC*, Milan, Italy, 2007, pp. 47–50.
- [16] E. Peiner, A. Schlachetzki, D. Krüger, "Doping profile analysis in Si by electrochemical capacitance-voltage measurements", *J. Electrochem. Soc.*, vol. 142, no. 2, pp. 576–580, 1995.
- [17] E. Lohmüller, S. Werner, B. Thaidigsmann et al., "The HIP-MWT+ solar cell concept on n-type silicon and metallization-induced voltage losses", *Proc. 29th EU PVSEC*, Amsterdam, Netherlands, 2014, this conference.
- [18] S. Solmi, A. Parisini, R. Angelucci et al., "Dopant and carrier concentration in Si in equilibrium with monoclinic SiP precipitates", *Phys. Rev. B*, vol. 53, no. 12, pp. 7836–7841, 1996.
- [19] A. L. Blum, J. S. Swirhun, R. A. Sinton et al., "An updated analysis to the WCT-120 QSSPC measurement system using advanced device physics", *Proc. 28th EU PVSEC*, Paris, France, 2013, pp. 1521–1523.
- [20] A. Drews, F. Clement, A. Spribille et al., "HIP-MWT solar cells - pilot-line cell processing and module integration", *Proc. 27th EU PVSEC*, Frankfurt, Germany, 2012.
- [21] H. Murrmann, D. Widmann, "Current crowding on metal contacts to planar devices", *IEEE Trans. Electron Devices*, vol. 16, no. 12, pp. 1022–1024, 1969.
- [22] B. Thaidigsmann, A. Wolf, F. Clement et al., "Combining the advantages of wrap through metallization and rear surface passivation into industrial MWT-PERC devices", *Proc. 25th EU PVSEC*, Valencia, Spain, 2010, pp. 2227–2230.